J. Biomechanics, 1973, Vol. 6, pp. 547–559. Pergamon Press. Printed in Great Britain

FLOW CHARACTERISTICS IN MODELS OF ARTERIAL STENOSES—II. UNSTEADY FLOW*

DONALD F. YOUNG†
Department of Engineering Mechanics and Biomedical Engineering Program, Iowa State University, Ames, Iowa 50010, U.S.A.

and

FRANK Y. TSAI‡
Department of Engineering Mechanics and Engineering Research Institute, Iowa State University, Ames, Iowa 50010, U.S.A.

Abstract—In Part I of this paper the effect of a stenosis on the steady flow through a tube was considered. In Part II the effect of unsteadiness is investigated experimentally using the same axisymmetric and nonsymmetric models. Oscillating flow, with and without a steady component, was utilized and the pressure drop was determined as a function of several parameters. An approximate equation for predicting the pressure drop across a stenosis is developed, and verified experimentally. It is shown that three dimensionless parameters can be used to characterize the unsteady flow in a stenosis.

Hot-film measurements were used to investigate the development of turbulence and it was found that the oscillating flow was more stable than the corresponding steady flow for mild constrictions. For the severely constricted models the oscillating flow was slightly less stable than for steady flow.

1. INTRODUCTION

THE APPLICABILITY of steady-flow tests to problems related to arterial blood flow is questionable since blood flow is distinctly pulsatile. In Part II of this paper the influence of unsteadiness on the flow through locally constricted tubes is considered. Three of the model stenoses described in Part I were used in the test program and the same hydrodynamic factors are considered, i.e. pressure drop, flow separation, and the development of turbulence. Due to the general complexity of unsteady flow the primary quantitative results are limited to pressure-drop characteristics, although both separation and turbulence phenomena were studied and are discussed.

To make the problem more tractable, harmonically oscillating flow, superimposed on a steady flow, was used in the experiments. Although the wave form for blood flow is not harmonic, the results obtained with this simpler type of flow reveal the salient differences between steady and unsteady flow in constricted tubes.

2. THEORETICAL CONSIDERATIONS

Unsteady flow in a straight tube

One of the simplest unsteady-flow problems of practical interest is that of harmonically oscillating laminar flow in a long tube of constant cross section containing a Newtonian incompressible fluid. An exact solution to this problem can be obtained from the Navier-Stokes equations and the results of this solution are readily available in the literature (see for example, Wormersley, 1955). Experimental verification of the theoretical solution has been obtained by Linford and Ryan (1965). The equations for the velocity distribution and the pressure gradient for a given flow rate

*Received 17 July 1972.
†Professor.
‡Assistant Professor.

are rather complicated and are commonly expressed in terms of Bessel functions. However, a very accurate approximation to the exact solution can be made which is particularly useful in giving a physical interpretation to the problem. Schönfeld (1949) has shown that at relatively low oscillation frequencies the pressure drop Δp over a length L can be predicted from the equation

$$\Delta p = \frac{32\mu L}{D^2} U + \frac{4}{3}\rho L \frac{dU}{dt}, \qquad (1)$$

where μ is the fluid viscosity, ρ the fluid density, D the tube dia., U the average instantaneous velocity, and dU/dt the time rate of change of the average velocity. The first term on the right side of equation (1) is the pressure drop due to viscous effects in steady flow and the second term is the additional pressure force required to accelerate the fluid. For the straight tube problem the parameter used as an index of the ratio of inertial to viscous effects is $\alpha = R_0\sqrt{\omega/\nu}$ where R_0 is the tube radius, ω the angular frequency of the oscillation, and ν the kinematic viscosity. Equation (1) is in good agreement with the exact solution for $\alpha < 3$. Fry *et al.* (1956, 1959) modified equation (1) to read

$$\Delta p = (1{\cdot}6)\left(\frac{32\mu L}{D^2}\right) U + (1{\cdot}1)\,\rho L \frac{dU}{dt}, \qquad (2)$$

where the constants 1·6 and 1·1 were determined empirically to give good agreement between experimental measurements and equation (2) in the study of aortic blood flow.

If equation (1) is written in the form

$$\Delta p = C_v\left(\frac{32\mu L}{D^2}\right) U + C_u \rho L \frac{dU}{dt}, \qquad (3)$$

the coefficients C_v and C_u can be calculated from the exact solution so that both the amplitude and phase angle between Δp and U is accurately predicted from equation (3). These calculated values are shown in Fig. 1 as a function of α. The values of C_v and C_u in equation (2) are approximately equal to the values obtained from the graph for $\alpha = 7$.

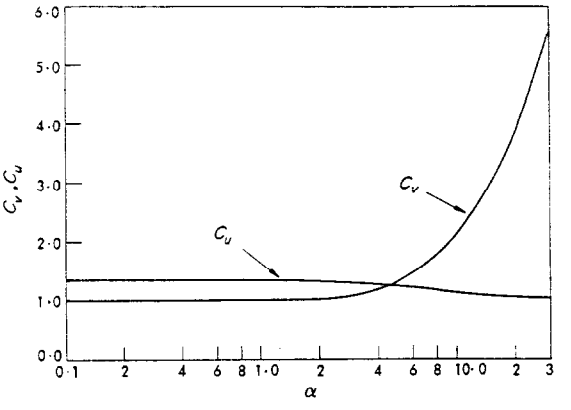

Fig. 1. Variation of coefficients C_v and C_u with α for oscillating flow in a straight tube.

Although C_v increases rapidly for large values of α the amplitude of Δp is dependent primarily on the inertia term for $\alpha > 10$, and variations in C_v are only important if an accurate prediction of the phase angle is required. Similarly for small α the pressure drop depends primarily on C_v; the value of C_u is relatively unimportant except for the phase relationship.

Momentum analysis

Although an analytical solution for the problem of unsteady flow in a constricted tube is not available due to the nonlinear nature of the flow and the turbulence which commonly develops near the constriction, a momentum analysis is useful for focusing attention on the various factors which enter the problem. A similar analysis was used by Daily *et al.* (1956) in their study of transient (but not oscillating) flow through orifices.

Consider a tube containing a constriction as shown in Fig. 2. Application of the linear momentum equation to the dashed control volume gives

$$\int_{A_0} p_1\,dA - \int_{A_0} p_2\,dA - F_b = \int_{A_0} \times \rho u_2^2\,dA - \int_{A_0} \rho u_1^2\,dA + \frac{\partial}{\partial t}\int_V \rho u\,dV, \qquad (4)$$

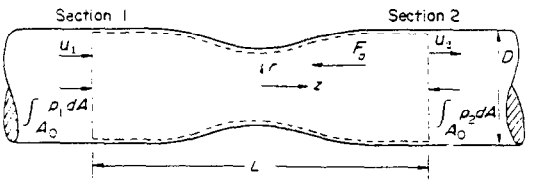

Fig. 2. Control volume for constricted tube.

where F_b is the resultant force exerted on the control volume by boundary forces, u is the local velocity in the z-direction, and V is the volume of fluid within the control volume. It is now assumed that sections 1 and 2 are sufficiently far away from the constriction so that $u_1 = u_2$ and the first two integrals on the right side of equation (4) cancel. The pressure integrals are expressed as

$$A_0 \Delta p = \int_{A_0} p_1 \, dA - \int_{A_0} p_2 \, dA,$$

where Δp represents the difference in the average pressure intensity at sections 1 and 2. Also the last integral can be written as

$$\frac{\partial}{\partial t} \int_V \rho u \, dV = \rho L \frac{dQ}{dt}$$

$$= \rho L A_0 \frac{dU}{dt},$$

where Q is the instantaneous discharge,

$$Q = \int_A u \, dA,$$

and U is the mean velocity in the unobstructed tube, i.e.

$$U = \frac{Q}{A_0}.$$

With these assumptions and simplifications equation (4) can be written as

$$\Delta p - \frac{F_b}{A_0} = \rho L \frac{dU}{dt}. \tag{5}$$

The boundary resistance term F_b contains the influence of viscosity, turbulence, and the pressure drag (added mass effect) due to the accelerated flow past the boundary. It is expected that this latter effect is proportional to the acceleration; and the influence of viscosity and turbulence to be closely related to that for steady flow. Thus, as a first approximation the boundary resistance is written as

$$\frac{F_b}{A_0} = \Delta p_{sf} + k \rho L \frac{dU}{dt},$$

where Δp_{sf} is the corresponding steady-flow pressure drop and k is some form of added mass coefficient. Thus, equation (5) can be written as

$$\Delta p = \Delta p_{sf} + (1 + k) \rho L \frac{dU}{dt}.$$

Finally, if the form of the equation developed in Part I for the steady-flow pressure drop is used it follows that

$$\Delta p = K_v \frac{\mu}{D} U + \frac{K_t}{2} \left[\frac{A_0}{A_1} - 1 \right]^2 \times \rho |U| U + K_u \rho L \frac{dU}{dt} \tag{6}$$

when the coefficient K_u has absorbed the added mass effect plus any correction to the viscous–turbulence terms that are proportional to dU/dt. Equation (6) for a straight tube reduces to the form of equation (3).

For the type of flow under consideration it is assumed that the instantaneous mean velocity can be expressed as

$$U = U_s + U_n f(\bar{t}), \tag{7}$$

where U_s is the steady component of velocity, U_n the peak unsteady component, $\bar{t} = t/\tau$ and τ is a characteristic time. The function $f(\bar{t})$ is assumed to be of a form such that the maximum values for both $f(\bar{t})$ and $df/d\bar{t}$ are

equal to unity. Equation (6) can now be written in the dimensionless form

$$\frac{\Delta p}{\rho U_P^2} = \frac{K_v}{\mathrm{Re}_p}\bar{U} + \frac{K_t}{2}\left[\frac{A_0}{A_1} - 1\right]^2 \times |\bar{U}|\bar{U} + \frac{K_u L U_n}{\tau U_p^2}\frac{df}{d\bar{t}} \qquad (8)$$

where U_p is the maximum velocity in the unobstructed tube ($U_p = U_s + U_n$), $\bar{U} = U/U_p$ and Re_p is the peak Reynolds number, $\rho D U_p/\mu$.

The relative importance of the three terms on the right side of equation (8) can be deduced by comparing the coefficients of the dimensionless variables $\bar{U}$, $|\bar{U}|\bar{U}$ and $df/d\bar{t}$ (all of which have maximum values of unity). These coefficients are denoted as I_v, I_t and I_u, i.e.

$$I_v = \frac{K_v}{\mathrm{Re}_p} \text{(index of viscous effects)}, \qquad (9)$$

$$I_t = \frac{K_t}{2}\left[\frac{A_0}{A_1} - 1\right]^2 \text{(index of turbulence effects)}, \qquad (10)$$

$$I_u = \frac{K_u L U_n}{\tau U_p^2} \text{(index of inertial effects)}. \qquad (11)$$

As noted in Part I the coefficient K_v is strongly dependent on the stenosis geometry (see Table 3, Part I). The coefficient K_t is approximately equal to unity, and for estimating orders of magnitude can be set equal to one. Also, K_u is expected to be of the order of unity.

The three parameters I_v, I_t and I_u can be used to estimate the relative importance of the various factors which contribute to the pressure drop in a stenosis. For example, in a severely constricted stenosis, I_t can easily be much larger than either I_v or I_u and the problem becomes a quasi-steady one in which the second term on the right side of equation (6) controls the pressure drop. For a mild stenosis with a highly accelerated flow (U_n/τ large), I_u can dominate and the pressure drop is due primarily to inertial effects. These parameters will be used in analyzing the experimental results described in the following sections.

For an oscillating flow in a straight tube ($I_t = 0$), the important dimensionless ratio becomes I_u/I_v, which is proportional to α^2 with $\tau = 1/\omega$. Thus, it is common practice to characterize oscillating flow in a pipe with the parameter α; i.e. for α small, viscous effects are dominant and the flow is quasi-steady whereas for α large, inertial effects are dominant. Although this single parameter is suitable for flow in unobstructed tubes it is clear for constricted tubes a single parameter will not suffice because of the additional parameter I_t.

3. EXPERIMENTAL APPARATUS AND PROCEDURES

Three of the model stenoses from the steady-flow tests were used in the unsteady flow tests. In particular, axisymmetric models M-1 (56 per cent stenosis) and M-2 (89 per cent stenosis) were used to investigate the effect of area ratio, and the nonsymmetric model M-5 (89 per cent stenosis) was used to study the effect of shape. The detailed description of these models is given in Table 1 of Part I.

The oscillating flow was generated by a piston-cylinder combination driven by a scotch-yoke mechanism. This apparatus combined with a steady-flow system similar to that used for the steady-flow tests made it possible to generate a harmonically oscillating flow superimposed on a steady flow component (see Fig. 3a). The scotch-yoke mechanism was driven by a variable-speed drive and was operated in a range of angular frequencies of about 5 rad/sec. The amplitude of the stroke could also be varied, and two different amplitudes were used in the tests. A general schematic of the flow system is shown in Fig. 3b. With valves A and B closed, the flow produced by the piston was a harmonic oscillation and the instantaneous flow rate could be

Table 1. Summary of test program

Test series designation	Fluid	Models used	Range of values for I_v	I_t*	I_u†
1S	Saline	M-1	0·1–0·4	0·8	2·3–17·0
2S		M-2	0·5–2·2	32·7	2·1–15·2
3S		M-5	0·9–4·8	32·7	2·2–19·4
1GS	Glycerol-saline	M-1	1·8–8·7	0·8	2·9–19·2
2GS		M-2	12·1–44·5	32·7	3·0–15·6
3GS		M-5	22·3–98·7	32·7	2·6–19·9

*With $K_t = 1{\cdot}0$.
†With $\tau = 1/\omega$ and $K_u = 1{\cdot}0$.

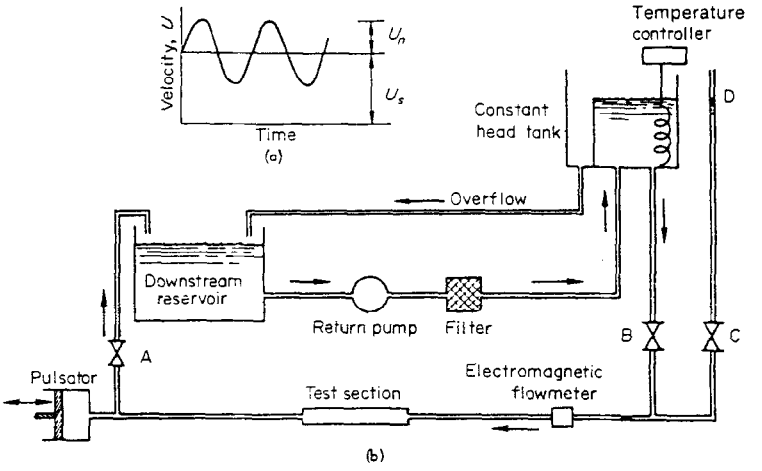

Fig. 3. Schematic of experimental apparatus.

obtained from a measurement of the piston position, the height of the oscillating vertical column of fluid at D, or from an in-line electromagnetic flowmeter (Biotronex Model BL-610) installed in the tube as shown. The flowmeter was calibrated immediately prior to the recording of data through the measurement of the oscillating column of fluid, and subsequently used for the instantaneous flow measurement.

In the test program two different fluids were used: physiological saline, and a glycerol-saline mixture (71 per cent glycerol by weight). The use of these two fluids made it possible to obtain a wide range in viscosity. Sodium chloride was added to the glycerol solutions to make them electrically conducting, and thus suitable for use with the electromagnetic flowmeter.

The pressure drop across the constricted tube was measured with two Statham P23Db pressure transducers whose outputs were electronically subtracted to give the instantaneous pressure drop. The transducers were connected to the same pressure ports used for the steady flow test by means of relatively short flexible connecting lines. The response characteristics of the flowmeter and pressure transducers were checked by taking measurements on a straight-tube test section and comparing the experimental data with the results predicted theoretically. The results were found to be in good agreement.

An attempt was made to study separation

phenomena by dye injections similar to the procedure used in the steady-flow tests. Due to the transient nature of the flow meaningful visual observations were difficult to make. Some exploratory work was done using high-speed photography, but interpretations of the complex flow patterns remained difficult and no quantitative results were obtained. However, a discussion of some of the qualitative features of the observed separation phenomena is given in a later section. Hot-film probes were used in a manner similar to that for the steady-flow tests to study the initiation of turbulence, and measurements were made at two locations downstream from the throat of the constriction ($z/Z_0 = 1$ and 4).

In planning the experimental program an attempt was made to cover a wide range of values for the parameters I_v, I_t and I_u. Table 1 gives a summary of the test program. For a given test series with a particular model and fluid the frequency ω was held constant and the steady-flow component U_s was varied from zero to its maximum value. The amplitude of the oscillating component U_n remained essentially constant for a given series. This procedure was repeated for a second value of U_n. It was not possible to hold I_u constant while varying I_v since both depended on U_p (ω and U_n could not be varied sufficiently to hold I_u constant with large variations in U_p).

A typical set of data for a given run is shown in Fig. 4. All data were recorded on a multichannel strip-chart recorder. The upper trace gives the velocity U as a function of time as recorded from the flowmeter. The trace immediately below the flowmeter recording is the corresponding pressure drop across the constriction and the last two traces are hot-film recordings at two downstream locations. Each test series designated in Table 1 consisted of 20–25 runs of this type. The flattening of the pressure-drop curve at two points during a cycle as shown in Fig. 4b is not an anomaly but is, in fact, predicted by the nonlinear term in equation (6).

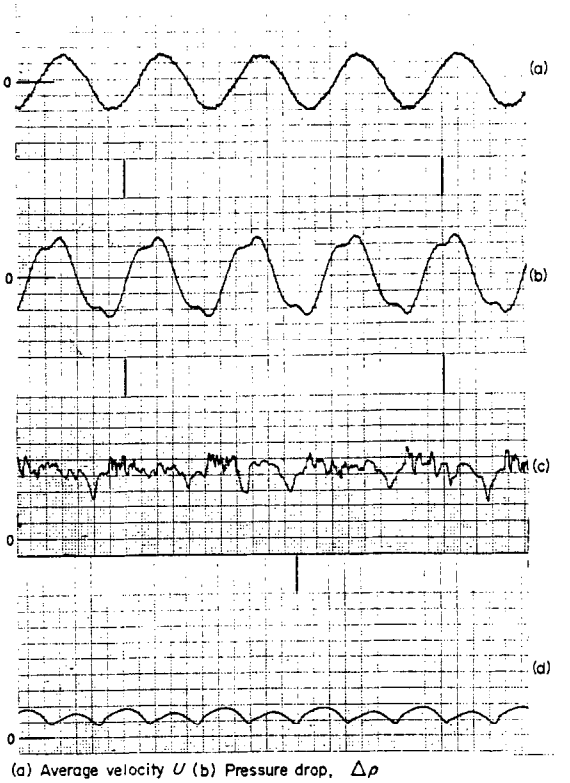

(a) Average velocity U (b) Pressure drop, Δp
(c) Hot-film probe at $z/Z_0 = 1$ (d) Hot-film probe at $z/Z_0 = 4$

Fig. 4. Typical experimental recordings.

4. RESULTS

Pressure drop

A typical pressure-drop wave form is shown in Fig. 5a for $U = U_n \cos \omega t$. The theoretically predicted pressure drop from equation (6) with $K_u = 1{\cdot}0$ is also shown in Fig. 5a. Immediately below in Fig. 5b is shown the contribution of the various components in equation (6). Although equation (6) is based on a very simplified analysis it does a reasonably good job of predicting the pressure drop—not only the peak values but the general shape of the wave form as illustrated in Figs. 5a and 6, in which several typical curves are shown. Differences between predicted and observed peak pressure drops were about 20 per cent or less. By adjusting the coefficients K_v, K_t and

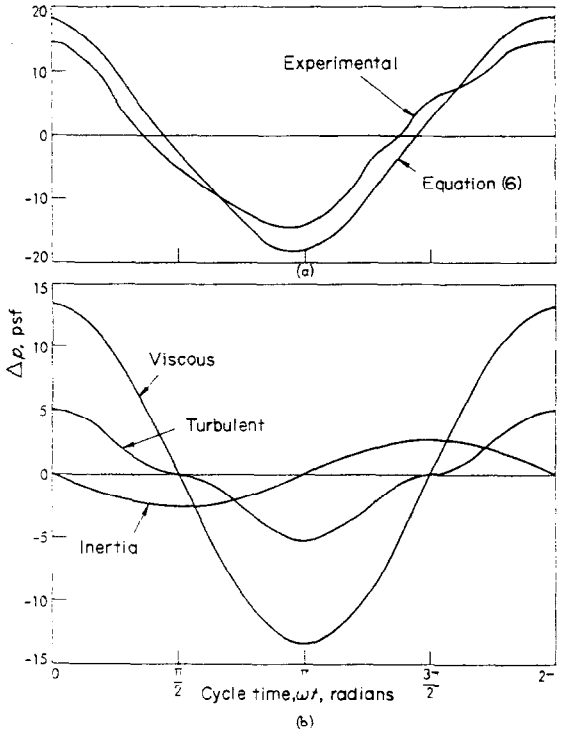

Fig. 5. Pressure-drop wave forms for model M-5 ($U_s = 0$; $Re_p = 76$).

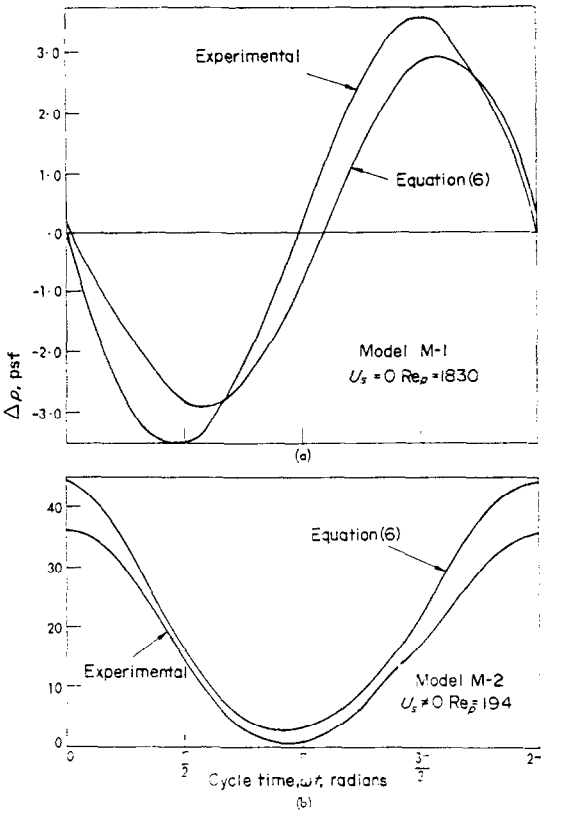

Fig. 6. Pressure-drop wave forms for models M-1 and M-2.

K_u this agreement could be considerably improved as discussed below.

For the tests with the severe constrictions (M-2 and M-5) the pressure drop is due primarily to viscous and turbulence effects $(I_v + I_t) \gg I_u$ and the problem is approximately quasi-steady. In this case the pressure drop is essentially in phase with the discharge as shown in Figs. 5a and 6b. A plot of the peak pressure drop which occurs during a cycle (in dimensionless form) versus the peak Reynolds number is shown in Figs. 7 and 8 for all tests run with models M-2 and M-5. Some of the plotted points represent multiple data points which essentially fall on top of one another. In general, the pressure drop is slightly lower for unsteady flow than for steady flow in this quasi-steady regime. It appears that although inertial effects are small, the development of separation and turbulence is delayed so that

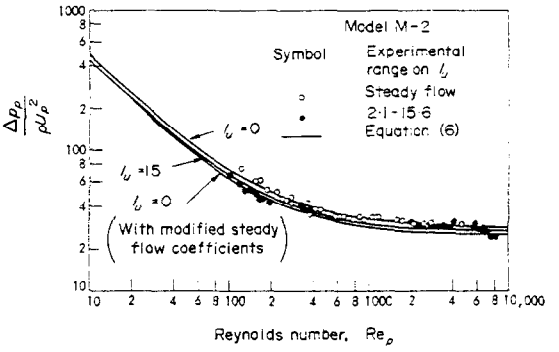

Fig. 7. Dimensionless peak pressure-drop versus peak Reynolds number for model M-2.

the resulting pressure drop is lower. For model M-2 it was found that if the coefficients K_v and K_t were reduced by about 10 per cent, an improved overall fit was obtained as shown

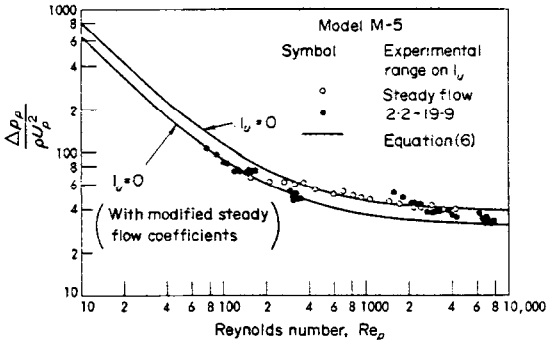

Fig. 8. Dimensionless peak pressure drop versus peak Reynolds number for model M-5.

in Fig. 7. For model M-5 a plot with K_v and K_t reduced by 20 per cent is shown in Fig. 8. The relative insensitivity of the peak pressure drop on the inertial term for these severely constricted models is illustrated in Fig. 7.

For the tests with the milder constriction (model M-1) inertial effects are important and for some of these tests $I_u \gg (I_v + I_t)$ and inertial effects are dominant. In this case, as predicted from equation (6), the dimensionless peak pressure drop will be a linear function of the parameter I_u. A plot of these data for M-1 for which $I_u/(I_v + I_t) > 3$ is shown in Fig. 9. Clearly a straight line having a slope of unity gives a good fit to these data. The intercept of the curve is approximately 1·2 which suggests that added mass effects plus variations in the flow patterns, which are functions of the acceleration, cause an increase in the coefficient K_u to 1·2 for model M-1. It should be emphasized that this coefficient is a function of stenosis geometry.

For those cases in which viscous, turbulence, and inertial effects are all important the pressure drop, for a given geometry, can be expressed as a function of the peak Reynolds number Re_p and I_u as shown in Fig. 10. Although in general the pressure drop will also depend on U_s/U_n, the effect of this ratio is negligible for all tests run ($0 < U_s/U_n < 2{\cdot}4$). For the curves shown in Fig. 10 the range of values of I_u (for $K_u = 1{\cdot}0$) are given on the figure. The solid lines plotted in

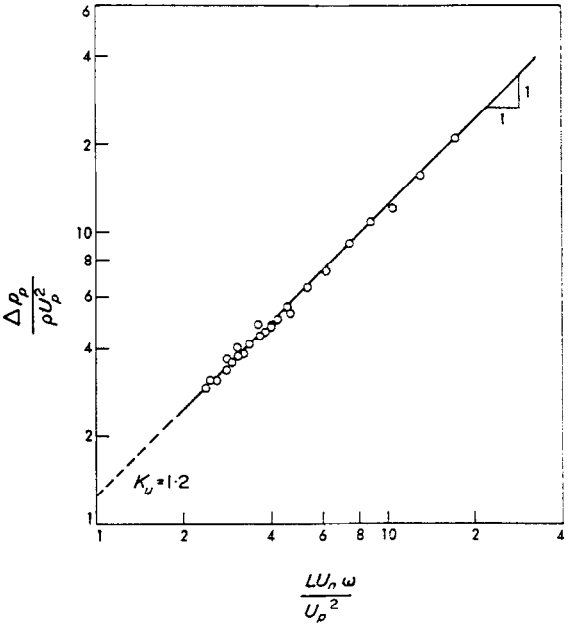

Fig. 9. Dimensionless peak pressure drop versus inertial parameter I_u for model M-1.

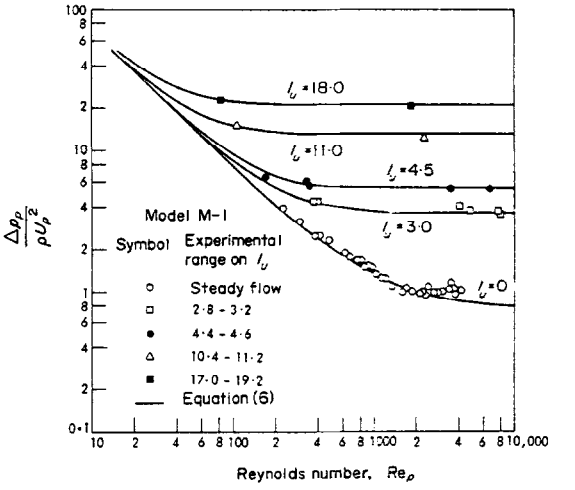

Fig. 10. Dimensionless peak pressure drop versus peak Reynolds number for model M-1.

Fig. 10 are obtained from equation (6) with $K_u = 1{\cdot}2$ and indicate the excellent agreement between this equation and the experimental data.

The results of this test program indicate that the parameters I_v, I_t and I_u can be used to

determine the various flow regimes which may be encountered in the unsteady flow in a stenosis. Furthermore, equation (6) can be used to estimate the pressure drop for a given discharge with the coefficients K_v and K_t obtained from steady-flow tests and K_u set equal to unity. The experiments have shown that these coefficients can be modified to obtain better agreement between theory and experiment. However, a precise evaluation of the coefficients will be difficult, since they are expected to be dependent on geometry, Reynolds number, U_s/U_n and I_u.

Separation

In the steady-flow tests described in Part I it was observed that as the Reynolds number exceeded some critical value, separation of the main stream from the boundary occurred and a localized zone of fluid containing a slowly recirculating mass of fluid could be detected. The same general phenomenon was observed in the unsteady-flow tests. However, for unsteady flow the quantitative description of the separation phenomenon is considerably more difficult to obtain since the position of separation and reattachments points are time dependent. Also, due to inertial effects, there is a phase difference between velocities at the same cross section so that at certain times during a cycle the velocity near the wall and in the central portion of the tube have different directions. This type of flow reversal is not considered as flow separation, which is generally thought of as a localized effect in which the flow reversal occurs over a limited length of the tube. And outside this localized region the flow near the wall is unidirectional. The combination of the general flow reversal induced by inertial effects and the localized flow reversal due to the convective acceleration induced by the constriction make it difficult to clearly delineate the separated flow regime. Although the results of these tests revealed that under certain conditions localized separated regions of flow existed for the unsteady flows, reliable quantitative data could not be obtained using visual observation. It appears that this aspect of the problem will require a more elaborate flow visualization scheme using high-speed photography.

Turbulence

To study the development of turbulence in the vicinity of the stenosis hot-film probes were inserted at two downstream locations ($z/Z_0 = 1$; $z/Z_0 = 4$). For flows which are laminar the output voltage from the hot-film, which can be related to the velocity, is smoothly varying as shown in the recordings of Figs. 11a, b and 12a. Since the output voltage is dependent on the magnitude of the velocity and not the direction the signals recorded are "rectified", and even with reversed flow the voltage does not change sign. It was also observed that the output signal for the hot-films never returned to the zero velocity baseline (indicated with a zero on the recordings) during a cycle even for reversed flow. Although not well understood it is thought that this anomalous behavior is due to some characteristic of hot-film probes when operating near the zero velocity point in an oscillating flow field.

Turbulence, or at least a highly disturbed flow, was initiated as some critical set of flow conditions was attained as illustrated in Figs. 11c and 12b. For some tests the flow was laminar over part of the cycle, became turbulent, with a subsequent return to laminar flow. This sequence of events can be clearly seen in Figs. 11c and 12b. As in steady flow it is difficult to determine accurately the critical Reynolds number for the initiation of turbulence since it is not known where along the tube turbulence first starts. Also, it is expected that the critical Reynolds number is dependent on the nature of the unsteadiness, as characterized by I_u and the ratio U_s/U_n. Some exploratory tests indicated that the radial position of the probe did not strongly influence the results.

For model M-1 turbulence was first detected at the probe position $z/Z_0 = 1$. However,

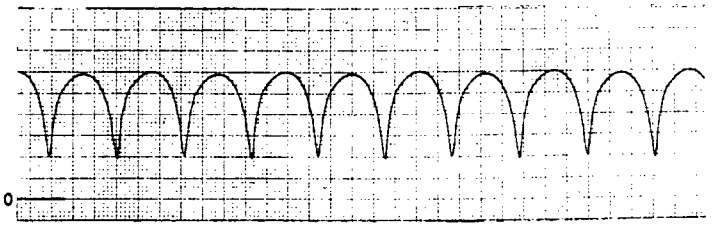

(a) Straight tube; $U_s = 0$; $Re_p = 2030$; Probe position at $r/R_0 = 0$

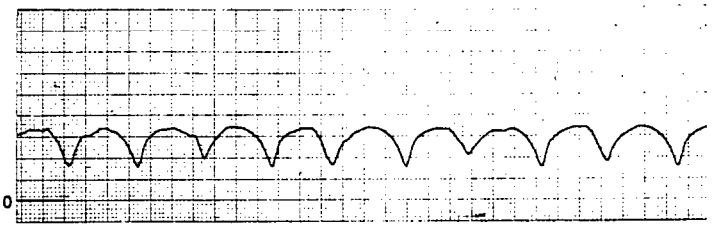

(b) Model M-1; $U_s = 0$; $Re_p = 1830$
Probe position at $z/Z_0 = 1$, $r/R_0 = 0.707$

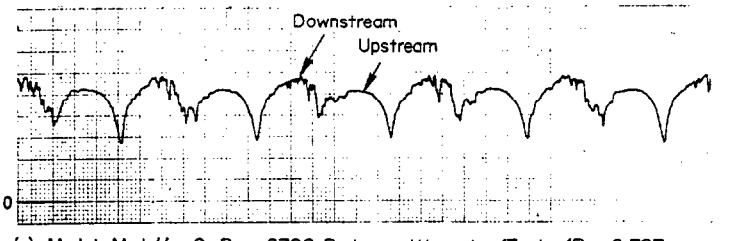

(c) Model M-1; $U_s = 0$; $Re_p = 6700$ Probe position at $z/Z_0 = 1$, $r/R_0 = 0.707$

Fig. 11. Typical hot-film recordings.

for the more severely constricted models, M-2 and M-5, turbulence was first detected at the downstream probe position, $z/Z_0 = 4$ as shown in Fig. 12. These results are consistent with those obtained in the steady flow tests. The "jetting" of the flow as it comes through a severely constricted model can be discerned in Fig. 12a where the velocity at the centerline is higher when the flow is in the downstream direction (flow from throat of constriction toward probe) than for the upstream direction, even though $U_s = 0$. Further downstream at $z/Z_0 = 4$ the 'jetting' has disappeared as shown in Fig. 12b.

Reynolds numbers at which turbulence was first detected are tabulated in Table 2. These data were obtained by examining a series of hot-film recordings and noting where the voltage first appeared to fluctuate significantly.

Table 2. Critical Reynolds numbers

Model	Unsteady flow			Critical Re_p for steady flow	
	Re_p	Turbulence observed	I_u	Transition	Turbulence
M-1	2330	No	10·4	300	500
	3500	Yes	4·6		
M-2	164	No	5·3	300	350
	323	Yes	4·9		
M-5	120	No	7·6	140	200
	173	Yes	2·6		

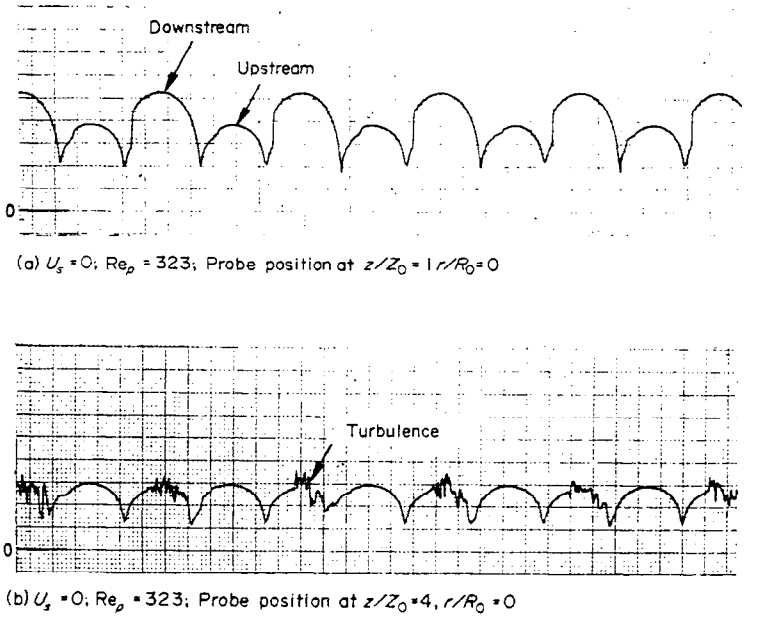

(a) $U_s = 0$; $Re_p = 323$; Probe position at $z/Z_0 = 1$ $r/R_0 = 0$

(b) $U_s = 0$; $Re_p = 323$; Probe position at $z/Z_0 = 4$, $r/R_0 = 0$

Fig. 12. Hot-film recordings for model M-2 at two downstream locations.

From a set of such recordings it was possible to determine a Reynolds number below which turbulence was not observed and above which turbulence was observed and thus bracket the critical Reynolds number. These limiting values are shown in Table 2 along with the corresponding values obtained in the steady-flow tests. Although no attempt was made to determine the effect of I_u on the critical Reynolds number corresponding values of I_u are included in the table. For model M-1 it appears that the initiation of turbulence is retarded by the pulsating flow. This result is consistent with observations in straight tubes (see, for example, Sarpkaya, 1966). In the straight tube studies the influence of α and U_n/U_s on the transition Reynolds number was considered and it was found for moderate values of α and U_n/U_s the critical Reynolds number was increased. Also, Gerrard (1971) found for pulsating turbulent flows in straight tubes that acceleration reduced the turbulent intensity but deceleration increased it. For the severely constricted models (M-2, M-5) turbulence appears to be initiated at a Reynolds number that is about the same, or slightly lower than the steady flow value.

5. SUMMARY

In the summary of Part I the results of the steady-flow tests were discussed with particular attention given to those hydrodynamic factors believed to have the greatest medical significance. This procedure is also followed here. It is to be noted that many of the results obtained from the steady flow tests are valid for unsteady flow but significant differences also exist.

(1) For unsteady flow in a constricted tube the three basic regimes of flow noted in steady flow are still discernible, i.e. laminar unidirectional flow, separated laminar flow, and turbulent flow. However, for an unsteady flow the existence of the various regimes is time-dependent and all three may be observed during one cycle of flow.

(2) It was found that the pressure drop across a stenosis could be approximated by the

relationship

$$\Delta p = K_v \frac{\mu}{D} U + \frac{K_t}{2}\left[\frac{A_0}{A_1} - 1\right]^2 \times \rho |U| U + K_u \rho L \frac{dU}{dt},$$

where the coefficients K_v and K_t were obtained from the steady-flow tests and $K_u \approx 1{\cdot}0$. Values of the peak pressure drop predicted on this basis agreed within about 20 per cent of the corresponding experimentally determined values for all tests. A much better agreement could be obtained with some empirical adjustments of the coefficients. In general it appears that K_v and K_t are reduced by the unsteadiness whereas K_u is greater than unity. A similar equation (equation 3) can be used for oscillating flow in a straight tube with C_v and C_u obtained from Fig. 1.

(3) Localized zones of separated flow were observed for the oscillating flows with time-dependent separation and reattachment points. However, quantitative results could not be obtained using visual observations.

(4) As the instantaneous Reynolds number increased during a cycle turbulence was observed if the Reynolds number exceeded a certain critical value. For Reynolds numbers slightly above this critical value the flow becomes turbulent and then returns to the laminar flow state prior to the beginning of the next cyclic increase in the Reynolds number. For the mildly constricted model (M-1) the critical Reynolds number was considerably larger than the corresponding value for steady flow. For the more severely constricted models the critical Reynolds numbers for steady and unsteady flow were comparable although lower for the unsteady flow (see Table 2). The downstream location at which the turbulence is initiated is strongly dependent on geometry.

(5) As was the case for steady flows the specific stenosis geometry is important in the quantitative prediction of flow characteristics. However, the more general qualitative aspects of the flow are independent of specific geometry. Equation (6) was found to be suitable for both the axisymmetric and nonsymmetric models.

(6) An analysis of equation (6) indicates that the unsteady flow can be characterized by the following three dimensionless parameters:

$$I_v = \frac{K_v}{\mathrm{Re}_p}$$

$$I_t = \frac{1}{2}\left[\frac{A_0}{A_1} - 1\right]^2 \quad (\text{with } K_t = 1{\cdot}0)$$

$$I_u = \frac{L U_n}{\tau U_p^2} \quad (\text{with } K_u = 1{\cdot}0)$$

(a) I_v is an index of purely viscous effects and K_v is strongly dependent on stenosis geometry. For an order of magnitude analysis the steady flow value of K_v can be used.

(b) I_t is an index of the importance of the nonlinear term in equation (6). Its presence is due to the convective acceleration which leads to flow separation and large turbulence losses.

(c) I_u is an index of inertial effects. The ratio U_n/τ represents the peak acceleration a_c so that $I_u = L a_c / U_p^2$ and the inverse of this parameter is sometimes referred to as an acceleration number.

These parameters can be used to estimate the relative importance of viscous effects, separation and turbulence, and unsteadiness.

Acknowledgments—The authors would like to thank Brian E. Morgan and Lawrence A. Davis, Jr. for their assistance in obtaining the experimental data, and Dr. Thomas R. Rogge for his help with the numerical computations. Special thanks are also due Dr. Neal R. Cholvin, Chairman of the Biomedical Engineering Program at Iowa State University, for many useful discussions related to the biomedical applications of this study. This work was

supported by the Engineering Research Institute, Iowa State University, through funds made available by Grant No. HE 11717 from the National Institutes of Health, U.S. Public Health Service.

REFERENCES

Daily, J. W., Hankey, W. L., Jr., Olive, R. W. and Jordaan, J. M. (1956) Resistance coefficients for accelerated and decelerated flows through smooth tubes and orifices. *Trans. ASME* **78**, 1071–1077.

Fry, D. L., Mallos, A. J. and Casper, A. G. T. (1956) A catheter tip method for measurement of the instantaneous aortic blood velocity. *Circ. Res.* **4**, 627–632.

Fry, D. L. (1959) Measurement of pulsatile blood flow by the computed pressure gradient. *Inst. Radio Engrs Trans. Med. Electronics* ME-6, 259–264.

Gerrard, J. H. (1971) An experimental investigation of pulsating turbulent water flow in a tube. *J. Fluid Mech.* **46**, 43–64.

Linford, R. G. and Ryan, N. W. (1965) Pulsatile flow in rigid tubes. *J. appl. Physiol.* **20**, 1078–1082.

Sarpkaya, T. (1966) Experimental determination of the critical Reynolds number for pulsating Poiseuille flow. *J. Basic Engr. Trans. ASME* **88**, 589–598.

Schönfeld, J. C. (1949) Resistance and inertia of the flow of liquids in a tube or open canal. *Appl. Sci. Res.* **A1**, 169–197.

Womersley, J. R. (1955) Method for the calculation of velocity, rate of flow and viscous drag in arteries when the pressure gradient is known. *J. Physiol.* **127**, 553–563.

NOMENCLATURE

a_c peak acceleration
A cross-sectional area
A_0 cross-sectional area of unobstructed tube
A_1 minimum cross-sectional area of stenosis
C_u inertial coefficient for straight tube equation
C_v viscous coefficient for straight tube equation
D dia. of unobstructed tube
F_b boundary force
I_t turbulence index $(A_0/A_1 - 1)^2 K_t/2$
I_u inertial index, $K_u L U_n/\tau U_p^2$
I_v viscous index, K_v/Re_p
k added mass coefficient
K_t turbulence coefficient
K_u inertial coefficient
K_v viscous coefficient
L distance between pressure taps
p pressure
Δp pressure drop
Δp_{sf} pressure drop due to steady flow
Q discharge
r radial coordinate
R_0 radius of unobstructed tube
Re_p peak Reynolds number, $\rho U_p D/\mu$
t time
u axial component of velocity
U instantaneous cross-sectional mean velocity in unobstructed tube
U_n amplitude of periodic component of cross-sectional mean velocity
U_p peak value of cross-sectional mean velocity, $U_p = U_s + U_n$
U_s steady component of cross-sectional mean velocity
$\bar{U}$ velocity ratio, U/U_p
z axial position from throat of stenosis
Z_0 half-length of stenosis
α alpha parameter, $R_0\sqrt{\omega/\nu}$
μ absolute viscosity
ν kinematic viscosity
ρ density of fluid
τ characteristic time
ω angular frequency of oscillating flow.